Enhanced Performance Consistency in Nanoparticle/TIPS Pentacene-Based Organic Thin Film Transistors

Zhengran He, Kai Xiao, William Durant, Dale K. Hensley, John E. Anthony, Kunlun Hong, S. Michael Kilbey II, Jihua Chen, and Dawen Li**

In this study, inorganic silica nanoparticles are used to manipulate the morphology of 6,13-bis(triisopropylsilylethynyl)-pentacene (TIPS pentacene) thin films and the performance of solution-processed organic thin-film transistors (OTFTs). This approach is taken to control crystal anisotropy, which is the origin of poor consistency in TIPS pentacene based OTFT devices. Thin film active layers are produced by drop-casting mixtures of SiO_2 nanoparticles and TIPS pentacene. The resultant drop-cast films yield improved morphological uniformity at ~10% SiO_2 loading, which also leads to a 3-fold increase in average mobility and nearly 4 times reduction in the ratio of measured mobility standard deviation (μ_{Stdev}) to average mobility (μ_{Avg}). Grazing-incidence X-ray diffraction, scanning and transmission electron microscopy as well as polarized optical microscopy are used to investigate the nanoparticle-mediated TIPS pentacene crystallization. The experimental results suggest that the SiO_2 nanoparticles mostly aggregate at TIPS pentacene grain boundaries, and 10% nanoparticle concentration effectively reduces the undesirable crystal misorientation without considerably compromising TIPS pentacene crystallinity.

1. Introduction

Solution-processed organic electronic devices are attractive because of their compatibility with solution-based low-temperature processing methods that could unlock the potential for low-cost, high-throughput fabrication over large areas on flexible substrates.[1–5] 6,13-bis(triisopropylsilylethynyl)-pentacene (TIPS pentacene) is a promising candidate for *p*-type organic thin-film transistor (OTFT) active layer because of its high mobility, air stability, and solution processibility.[6–11] However, TIPS pentacene crystalline films are highly anisotropic, which leads to significant variations in device performance.[12,13] In order to address this problem, polymer/TIPS pentacene blends have been used to improve film uniformity and reduce crystal misorientation. For example, Ohe et al. and Kang et al. blended poly(α-methylstyrene) (PαMS) with TIPS pentacene.[14,15] Enhanced performance reproducibility in PαMS/TIPS pentacene OTFTs was achieved due to vertical phase separation of the polymer and the small molecule organic semiconductor. Mobilities of 0.12 $cm^2\ V^{-1}\ s^{-1}$ and 0.3 $cm^2\ V^{-1}\ s^{-1}$, respectively, were reported[14,15] using a bottom-contact configuration. In addition, Smith et al. and Hamilton et al. blended an amorphous p-type polymer, poly(triaryl amine) (PTAA), with TIPS pentacene and successfully combined the good film-forming characteristics of PTAA and the high mobility of TIPS pentacene in OTFT devices.[16,17] More detailed aspects of acene-polymer and other solution-processed semiconducting blends were thoroughly covered in a recent review by Smith, et al.[18]

In this paper, we investigate the effect of nanoparticles, instead of polymer additives, on TIPS pentacene crystallization and OTFT performance. Nanoparticles have been shown to reduce crystallinity and crystal sizes in poly(ethylene oxide)/lithium salt systems,[19] but are barely explored in small molecule OTFT systems as far as we know. SiO_2 nanoparticles rather than metal nanoparticles are used for morphological tuning because in ideal situations (i.e. without moisture absorption) insulating nanoparticles should not cause additional leakage current in the OTFT channel. Phase separation in blends of TIPS pentacene and additive materials is largely dominated by TIPS pentacene crystallization, instead of mixing free energy in liquid states,[14–18] which suggests that modifying TIPS pentacene crystallization with nanoparticle additives may have useful and important impact on TIPS pentacene based organic thin-film transistors.

In this study, we used X-ray diffraction and optical microscopy to investigate thin film morphology of nanoparticle/TIPS pentacene blends, top-contact OTFTs to determine device

Z. He, W. Durant, Prof. D. Li
Department of Electrical and Computer Engineering
Center for Materials for Information Technology
University of Alabama
Tuscaloosa AL 35487, USA
E-mail: dawenl@eng.ua.edu
Dr. K. Xiao, D. K. Hensley, K. Hong, J. Chen
Center for Nanophase Materials Sciences
Oak Ridge National Laboratory
Oak Ridge, TN 37831, USA
E-mail: chenj1@ornl.gov
Prof. J. E. Anthony
Department of Chemistry
University of Kentucky
Lexington, KY 40506, USA
Prof. S. Michael Kilbey II
Center for Nanophase Materials Sciences
Oak Ridge National Laboratory
Oak Ridge, TN 37831, USA
Department of Chemistry
University of Tennessee
Knoxville, TN 37996, USA

DOI: 10.1002/adfm.201002656

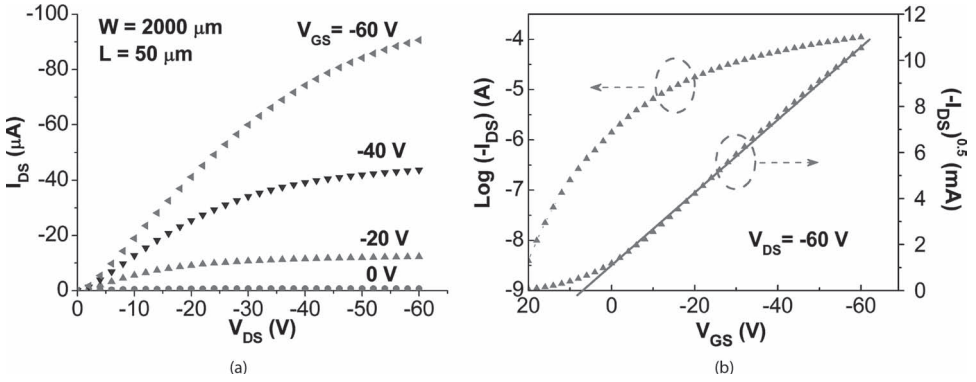

Figure 1. Typical output (left) and transfer characteristics (right) of SiO_2 nanoparticle/TIPS pentacene OTFTs. The shown device has a SiO_2 concentration of 10% by weight. The measured saturation mobility is 0.1 $m^2 V^{-1} s^{-1}$, with a threshold voltage of 8 V and on/off ratio above 10^4.

performance, and TEM to image crystal edges. According to our X-ray diffraction and optical microscopy, 10% SiO_2 nanoparticles can appropriately reduce the TIPS pentacene crystal width and enhance crystal orientation without significantly compromising the crystallinity. This results in considerably improved average mobility and performance consistency of TIPS pentacene OTFTs. Finally, TEM images show a much darker and broader TIPS pentacene crystal edge after nanoparticle incorporation, which provides evidence for nanoparticle aggregation at TIPS pentacene grain boundaries. Overall, this work demonstrates that nanoparticle addition provides a novel means to mediate the crystallization of solution processed small molecule organic semiconductor and may be used to effectively reduce the performance variation of solution-based organic thin-film transistors.

2. Results and discussion

A bottom-gate, top-contact, OTFT configuration is adopted throughout this work, with 250 nm thermal oxide gate insulator. Channel width and length are 2000 and 50 micrometers, respectively. **Figure 1** shows typical output and transfer characteristics of OTFTs with 10% SiO_2 nanoparticles in TIPS pentacene. From the fitted line in the square root plot of transfer characteristics, the saturation mobility is determined to be 0.1 $cm^2 V^{-1} s^{-1}$, and threshold voltage (V_T) is approximately 8 V. From the plot in the lograthmic scale, on/off ratio is estimated to be 10^4–10^5. Transfer characteristics were measured 3 times in air and gave very consistent readings. The slight nonlinearlity close to the origin of the output curves is caused by the intrinsic resistance of drop-cast TIPS pentacene active layer in a top contact, bottom gate OTFT configuration.[20]

Measured mobility variation of SiO_2 nanoparticle/TIPS pentacene OTFTs is compared with that of the devices based on pure TIPS pentacene, as shown in **Figure 2**. For devices with 0%, 2%, 5% and 10% SiO_2 nanoparticles, 10–20 devices were fabricated, while 6 devices were made for the OTFTs with 15% SiO_2 nanoparticles. The measured mobility variation of 10% SiO_2 devices is significantly less than that measured for OTFTs made of pure TIPS pentacene, as shown in Figure 2a. OTFTs based on pure TIPS pentacene exhibit field-effect mobilities varying by six orders of magnitude (ranging from 1.6×10^{-1} to 3.1×10^{-6} $cm^2 V^{-1} s^{-1}$), while the mobilities of TIPS pentacene OTFTs with 10% SiO_2 nanoparticles are consistently between 2.1×10^{-1} and 6.5×10^{-2} $cm^2 V^{-1} s^{-1}$. The mobilities of pure TIPS pentacene obtained in this work are comparable to those measured in earlier work.[12,15] Park et al. reported hole mobilities of 0.65 ± 0.35 $cm^2 V^{-1} s^{-1}$ in solution processed TIPS pentacene OTFT with a bottom-contact configuration and hexamethyldisilazane (HMDS) treatment on gate dielectrics, and their highest measured mobility (1.8 $cm^2 V^{-1} s^{-1}$)[10]

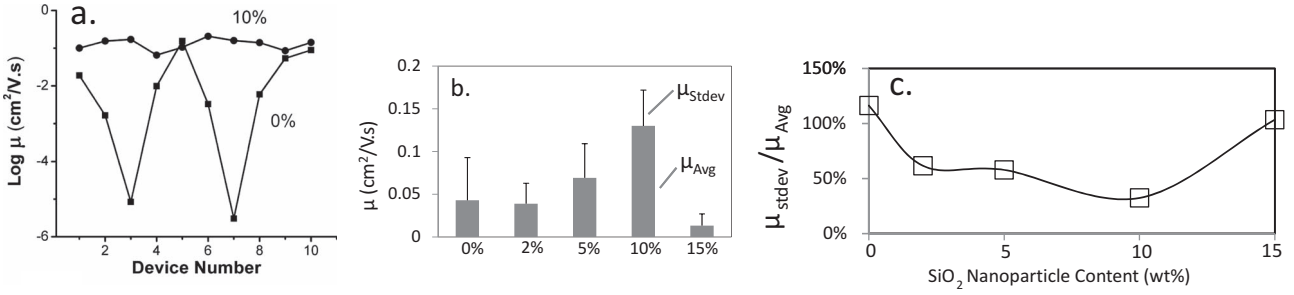

Figure 2. Mobility variation of SiO_2 nanoparticle/TIPS pentacene OTFTs as compared to that of the devices based on pure TIPS pentacene. a) The mobility variation of 10% SiO_2 devices is significantly less than that of pure TIPS pentacene OTFTs as shown in logarithmic scale. b) Measured standard deviation and average mobility as a function of SiO_2 content. The error bands stand for the standard deviation of measured mobilities (μ_{Stdev}), while the solid bars represent the measured average mobilities (μ_{Avg}). c) The ratio of standard deviation to measured average mobility as a function of SiO_2 content.

is one order of magnitude higher than the highest mobility that we measured (0.16 $cm^2\ V^{-1}\ s^{-1}$). Nevertheless, we believe that our OTFT configuration is more optimized for studying the effect of nanoparticle addition because a TIPS pentacene/SiO_2 nanoparticle solution severely dewets on HMDS treated substrate, resulting in poor film coverage. In Figure 2b, the measured average mobility and standard deviation of SiO_2 nanoparticle/TIPS pentacene OTFTs are plotted as a function of SiO_2 nanoparticle content. The average mobility increases as the concentration of SiO_2 nanoparticles initially increases from 0% to 2%, 5%, reaching a maximum at 10%. However, the average mobility drops when the concentration of SiO_2 nanoparticles is increased further to 15% as indicated in Figure 2b. The ratio of standard deviation to measured average mobility, which may be a more proper indicator of OTFT performance consistency, is shown in Figure 2c. Among all devices studied, OTFTs with 10% SiO_2 nanoparticles show the lowest performance variation and the highest average mobility. The ratios of measured mobility standard deviation (μ_{Stdev}) to average mobility (μ_{Avg}) for other nanoparticle concentrations (in the range of 0–15%) are up to 3 times higher than that of devices with 10% nanoparticles. At the same time, the average mobility of TIPS pentacene OTFTs is increased from 0.04 ± 0.04 $cm^2\ V^{-1}\ s^{-1}$ with 0% SiO_2 to 0.13 ± 0.04 $cm^2\ V^{-1}\ s^{-1}$ with 10% SiO_2. The average mobility measured for devices with 2%, 5%, and 15% nanoparticles is 0.04 ± 0.02 $cm^2\ V^{-1}\ s^{-1}$, 0.07 ± 0.04 $cm^2\ V^{-1}\ s^{-1}$, and 0.01 ± 0.01 $cm^2\ V^{-1}\ s^{-1}$ respectively. These mobilities are 2–10 times lower than that of devices with 10% nanoparticles. Based on our data, no strong dependence on nanoparticle concentration was observed for threshold voltages and on/off ratios of devices with 0–15% SiO_2.

To further understand the measured OTFT mobility behavior, both polarized optical microscopy (**Figure 3**) and grazing-incidence X-ray diffraction (**Figure 4**) were used to study the crystal orientation and crystallinity of SiO_2 nanoparticles/TIPS pentacene thin films. As shown in Figure 3, the color variation of polarized light microscopy images results from both crystal orientation and thickness. The needle-shaped TIPS pentacene domains are highly crystalline with the acene-ring lying "edge-on" to the substrate.[21,22] The long axis of the needle-shaped crystalline domains is [210], while the short axis is [$1\bar{2}0$].[23–25] As seen in Figure 3, the pure TIPS pentacene thin films are highly anisotropic with large variations in the grain width (the short axis of the needle-shaped crystals) and crystal orientation, which corresponds to measured mobilities varying widely from 1.6×10^{-1} to 3.1×10^{-6} $cm^2\ V^{-1}\ s^{-1}$. When the concentration of SiO_2 nanoparticles is increased to 5–10%, TIPS pentacene crystals have a smaller average grain width and a more uniform grain size distribution. From 10 measurements

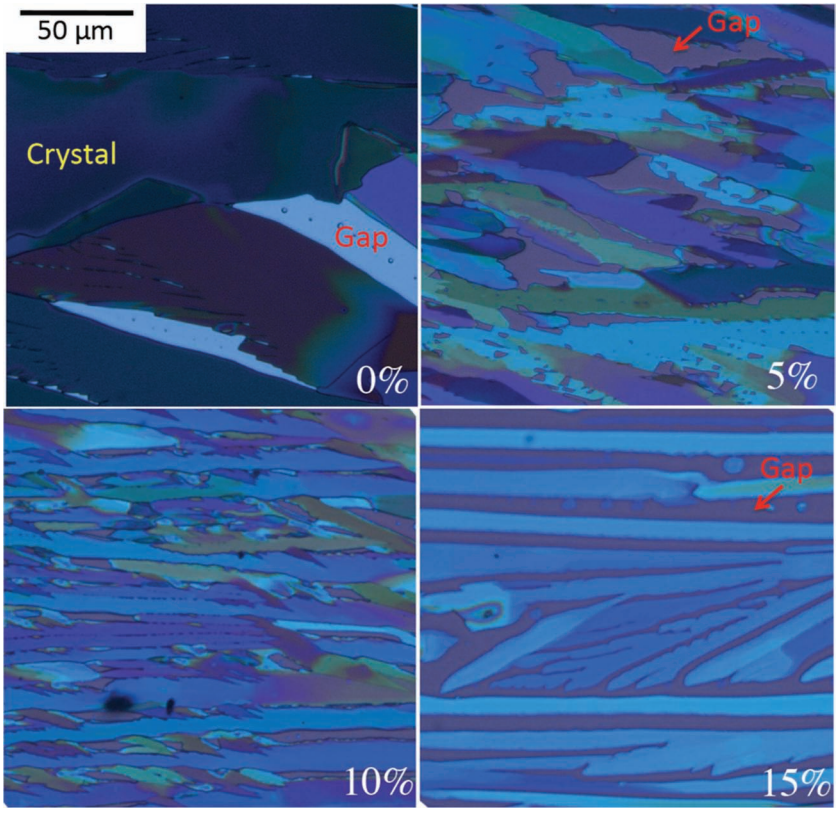

Figure 3. Polarized optical microscopy images of drop-cast TIPS pentacene films with SiO_2 concentrations of 0%, 5%, 10%, and 15%. All images share the same scale bar, which is shown at the top left.

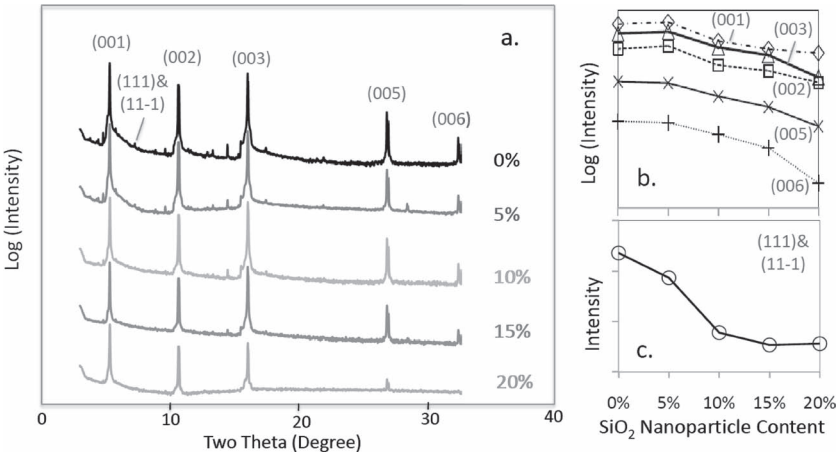

Figure 4. Grazing-incidence X-ray diffraction of TIPS pentacene films with different SiO_2 nanoparticle loading. a) The films exhibit consistent (*00l*) type reflections. b) The crystallinity of TIPS pentacene films decrease as the SiO_2 nanoparticle content increase beyond 5% as indicated by the reduced intensities of (*00l*) type reflections. c) The intensity of the combined peak of (111) and ($11\bar{1}$) plateaus after the nanoparticle concentration reaches 10%.

on crystal size in optical microscopy, the grain width of pure TIPS pentacene films is 42 ± 24 μm, and with 10% nanoparticle, the value is reduced to 11 ± 4 μm. On the other hand, the TIPS pentacene crystal orientation is enhanced at the expense of reduced grain width at an intermediate SiO_2 loading (~10%), as indicated in Figure 3. These films had the highest average mobility and lowest performance variation (Figure 2b and c). As the SiO_2 concentration is increased to 15%, nanoparticle aggregation becomes dominant, leading to circular-shaped small crystals and large gaps between TIPS pentacene "needles". The grain width of needle-shaped domains is reduced to 8 ± 3 μm (based on 10 measurements).

Grazing-incidence X-ray diffraction results from TIPS pentacene films with different SiO_2 nanoparticle loadings are shown in Figure 4a. The curves consistently exhibit strong (*00l*) type reflections, which match results reported previously for TIPS pentacene films.[8] In Figure 4a, the curves corresponding to different nanoparticle concentrations are shifted vertically to enable comparison. It is noted that the crystallinity of TIPS pentacene films decreases as the SiO_2 nanoparticle content increases at SiO_2 nanoparticle loadings above 5%, as indicated by the intensity decrease of (*00l*) type reflections (Figure 4b). Besides the intense (*00l*) reflections reported in literature,[8] we also noted many fine peaks in films with 0–5% SiO_2 at 2θ of 5°–25° that are not of (*00l*) type (Figure 4a). For example, the combined peak of (111) and $(11\bar{1})$ is visible in XRD results with 0–5% SiO_2. As the SiO_2 content increases to 10% and higher, this peak decreases significantly and then plateaus (Figure 4c). For X-ray diffraction patterns of a TIPS pentacene single crystal through *ac* and *bc* planes, the combined peak of (111) and $(11\bar{1})$ will not be present according to our X-ray simulation; thus, to some extent, we may use this combined peak to represent the misorientation of TIPS pentacene films. With the information from both optical microscopy and X-ray diffraction, we conclude that a balance of film connectivity, high crystallinity, and crystal orientation is achieved in devices with 10% SiO_2. Films with higher nanoparticle concentration have poor film connectivity and low crystallinity, while lower SiO_2 content yields higher crystallinity but poor crystal orientation.

To investigate the microstructural arrangement in SiO_2 nanoparticle/TIPS pentacene films, bright field TEM images were taken for the blend film, pure TIPS pentacene film and the nanoparticles, respectively (**Figure 5**). Regions of darker color (i.e., smaller gray value in Figure 5d) represent TIPS pentacene films or SiO_2 nanoparticles, while the lighter region (i.e., higher gray value in Figure 5d) corresponds to amorphous-carbon supporting films. Although it was not possible to visualize individual nanoparticles in the blend because of their aggregation, TEM images did show a distinctively darker and broader edge for TIPS pentacene films with 10% SiO_2 nanoparticles

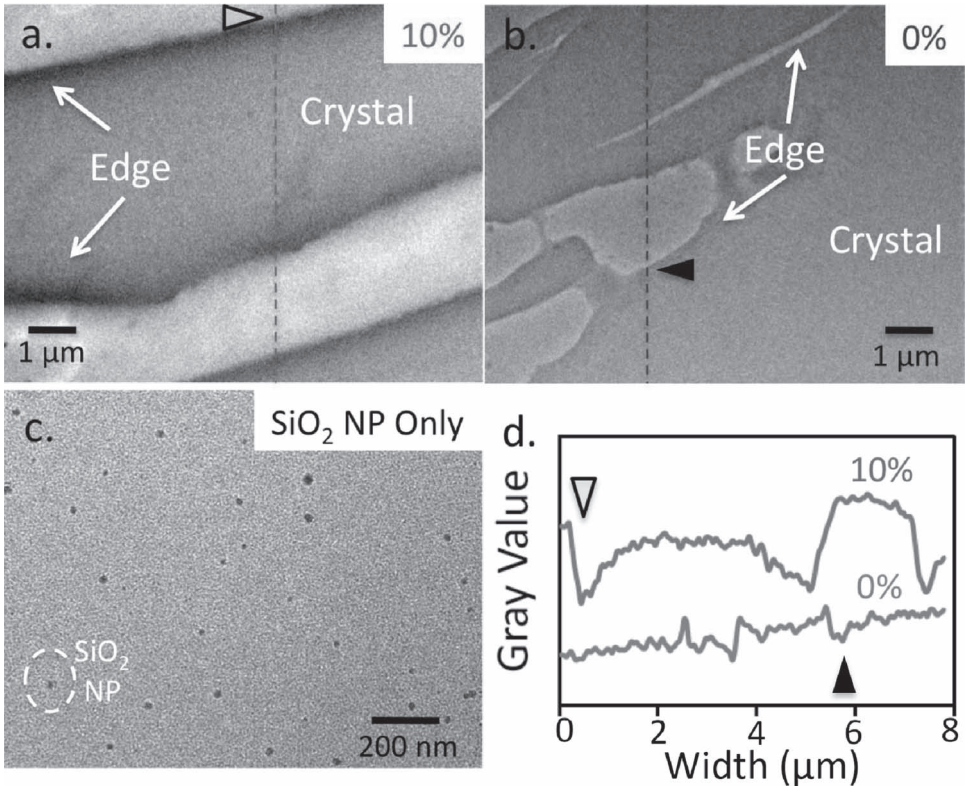

Figure 5. Bright-field TEM images show a distinctively darker and broader edge for TIPS pentacene films with a) 10% SiO_2 nanoparticles than that of b) the neat TIPS pentacene films. The freestanding SiO_2 nanoparticles are shown in (c). d) Two grayness curves are compared: a line corresponds to TIPS pentacene film with 10% nanoparticles (obtained from the dotted line shown in (a) and a line corresponds to the gray value obtained from pure TIPS pentacene film (at the dotted line shown in (b). Triangles shown in (a) and (b) mark the crystal edges, corresponding to the marked positions in the gray value curves (d).

(Figure 5a) than that of the neat TIPS pentacene films (Figure 5b). Pure SiO_2 nanoparticles are shown in Figure 5c, and the diameters of these particles are 18 ± 4 nm based on 12 different measurements. It is noted that the darker edge of the blend film is not a result of defocus or crystal topography, as it appears consistently in different SiO_2/TIPS pentacene crystals. The inner part of SiO_2/TIPS pentacene film is rather uniform in terms of electron contrast, while the gray value gradient of the film edge is very likely caused by aggregation of nanoparticles at grain boundaries, which is responsible for the changes that we observed in optical microscopy images (Figure 3). To quantitatively compare the film edges, a grayness plot is presented in Figure 5d. The two triangles in Figure 5a and 5b each mark a crystal (or film) edge, corresponding to the two marked edge positions in grayness curves (Figure 5d). The width of the film edge with 10% nanoparticles is about 1.5 μm, while that of the pure TIPS pentacene film is only 0.2 μm. Because this edge width analysis is based on the gray value derived from the TEM image, it is not clear if the nanoparticles are located on top of the edge or inside TIPS pentacene crystals. A previous report confirmed that molecular orientation of TIPS pentacene on amorphous carbon substrate is identical to that on an oxidized silicon wafer.[13]

Since the semiconductor–insulator interface is most critical to thin-film transistor operation and vertical separation plays a significant role in TIPS pentacene/polymer binder systems,[14–18] we performed low-voltage cross-sectional SEM for TIPS pentacene blend film with 10% SiO_2 nanoparticles. A charge compensation mode was used at 0.5 kV to effectively avoid charging effects from TIPS pentacene. Round-shaped silicon dioxide nanoparticles with ~20 nm diameters are visible in typical low-voltage SEM images (**Figure 6**a). The vertical distribution of SiO_2 nanoparticles in TIPS pentacene film is presented in Figure 6b. A total of 45 nanoparticles were sampled from different SEM images at different regions. In Figure 6b, Z is defined as the distance from the center of a nanoparticle to the gate insulator surface. The plot of nanoparticle percentage as a function of relative vertical position clearly demonstrates that the nanoparticles are mostly concentrated in the central region of the active layer (Z/Film Thickness = 20–80%). Since most nanoparticles are located away from the semiconductor/insulator interface, we do not expect that the addition of SiO_2 nanoparticles will significantly deteriorate charge transport in the channel.

Based on our diffraction and microscopy results, the TIPS pentacene crystalline films do not change their crystal structure or unit cell upon nanoparticle addition. Instead, the nanoparticles settle at the grain boundaries of TIPS pentacene crystals, effectively modifying film anisotropy as sketched in **Figure 7**. With the reduced grain width at 10% SiO_2, it is easier for the TIPS pentacene crystals to grow and organize along a uniform direction. This in turn leads to more consistent OTFT performance; however, too high of a nanoparticle concentration seems to reduce the TIPS pentacene crystallinity and grain size, which leads to poorer OTFT performance.

The nanoparticles that we used in this work are highly hydrophilic in nature as they have many hydroxyl groups on nanoparticle surface. This may not be ideal for OTFT application because of the possibilities of moisture absorption and enthalpically unfavored interactions with TIPS pentacene. Further work could be done to modify the nanoparticle surfaces with polymers and organic ligands with different hydrophobicity. By making

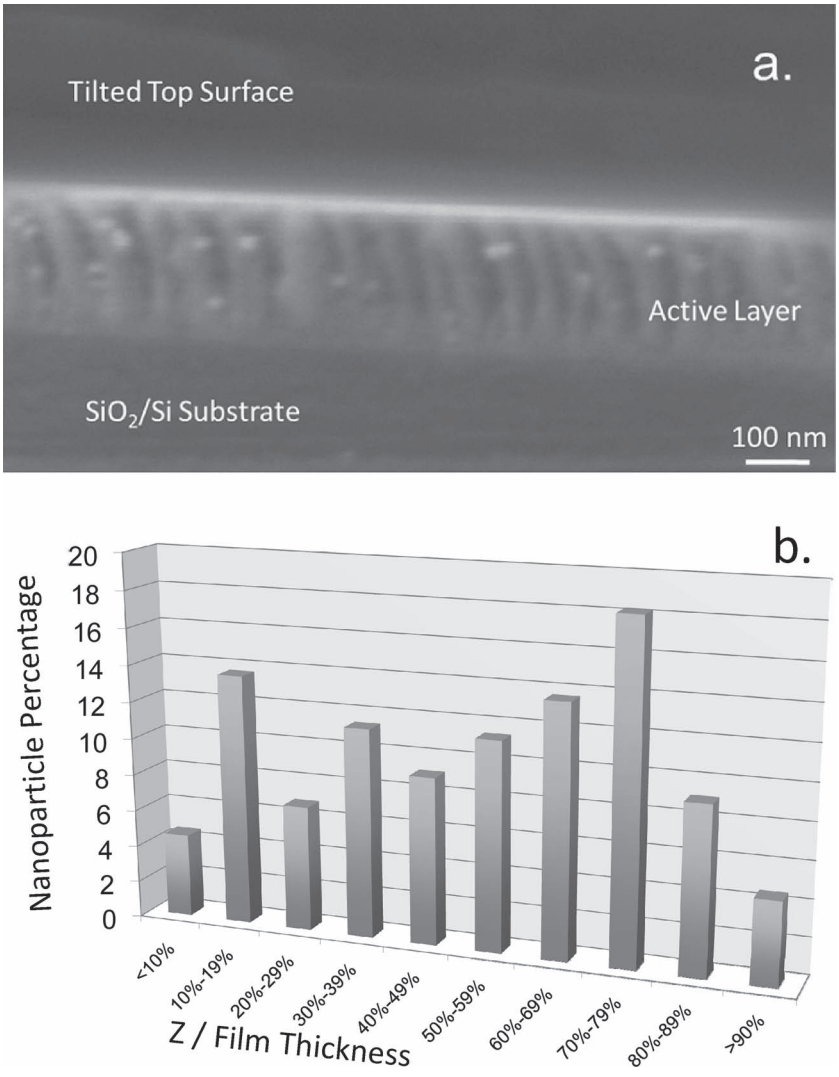

Figure 6. Vertical distribution of SiO_2 nanoparticles in TIPS pentacene active layer. a) A typical cross-section SEM image of TIPS pentacene with 10% SiO_2 nanoparticles loading. b) Vertical distribution of nanoparticles in TIPS pentacene blend with 10% SiO_2 nanoparticles. Z is the distance between the center of a nanoparticle and the semiconductor/dielectric interface. Only 4% SiO_2 nanoparticles are close to the TIPS pentacene/SiO_2 insulator interface (Z/Film Thickness < 10%).

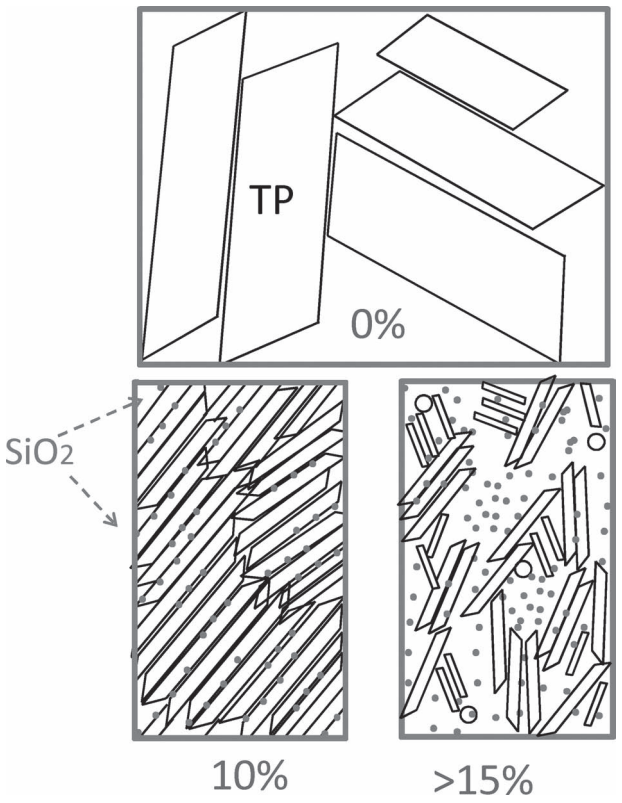

Figure 7. Sketches representing TIPS pentacene films with different SiO_2 nanoparticle concentration."TP" stands for TIPS pentacene crystals.

the surfaces less hygroscopic and tuning the polarity of nanoparticle surfaces, it may be possible to better mediate thin film morphologies and crystallization of solution-processible small molecule organic semiconductors for OTFT applications.

3. Conclusions

The OTFTs based on SiO_2 nanoparticles/TIPS pentacene show enhanced performance consistency marked by increases in average mobility and reduction of mobility standard deviation (μ_{Stdev}) to average mobility (μ_{Avg}) ratio in comparison to OTFTs made from neat TIPS pentacene. At 10% SiO_2 concentration, the measured hole mobility is 0.13 ± 0.04 cm^2 V^{-1} s^{-1} while the corresponding OTFTs made from neat TIPS pentacene have a mobility of 0.04 ± 0.04 cm^2 V^{-1} s^{-1}. TEM images reveal that the edges of TIPS pentacene crystals with 10% SiO_2 are significantly darker and about 8 times wider than that of pure TIPS pentacene films, which is likely caused by nanoparticle aggregation at TIPS pentacene grain boundaries. Both polarized optical microscopy images and X-ray diffraction results demonstrate that, with 10% SiO_2 nanoparticles, improved crystal orientation is achieved while maintaining relatively high level of TIPS pentacene crystallinity.

4. Experimental Section

Materials and Thin Film Formation: TIPS pentacene was synthesized according to an earlier publication.[6] SiO_2 nanoparticles (nominally 20 nm diameter, purchased from Sigma Aldrich) are highly hygroscopic because of their hydrophilic surfaces and extremely high surface-to-volume ratio. Before blending in solution, SiO_2 nanoparticles were baked in an oven at 160 °C for 2–3 days to drive out absorbed moisture. We found this step is crucial, as TIPS pentacene solutions with moisturized nanoparticles will be more likely to dewet on oxide substrates. Dry SiO_2 nanoparticles were first dispersed in anhydrous toluene with ultra-sonication for 1 h, and then mixed with a pre-made TIPS pentacene solution (with anhydrous toluene) at different concentrations to yield solutions having specific nanoparticle loadings ranging from 0 to 20 wt%. A constant total solid concentration (~5 mg ml^{-1}) was maintained. SiO_2 nanoparticle/TIPS pentacene thin films are subsequently formed by drop casting in a solvent rich environment.[10] A small tilt angle of less than 5° was used to facilitate crystal orientation and keep the film thickness uniform over the substrate.

Device Fabrication and Characterization: A bottom-gate, top-contact configuration is used throughout this study. Heavily doped n-type Si substrates serve as the bottom gate contacts, and 250-nm-thick thermal oxide layers function as gate insulators (specific capacitance: 13.8 nF cm^{-2}). After drop-casting, a gold layer of 50 nm thickness was subsequently deposited through a shadow mask to form the source and drain contacts. The electrode deposition was performed in a thermal evaporator (Angstrom Engineering) at 10^{-7} Torr using a deposition rate of 0.5–1 Å s^{-1}. The electrical performance of OTFTs, including transistor transfer (I_{DS}–V_{GS}) and output (I_{DS}–V_{DS}) characteristics, was measured with a Keithley 4200 semiconductor parameter analyzer. All measurements were made at ambient conditions at room temperature. From the slope of the transfer characteristics $(I_{DS})^{1/2}$– V_{GS}, field-effect mobility in the saturation regime (V_{DS} = –60 V) was extracted based on the traditional MOSFET equation:

$$I_{DS} = \mu C_i \frac{w}{2L}(V_{GS} - V_T)^2 \quad (1)$$

where μ is the saturation mobility, C_i is the specific capacitance of gate insulator, L is the channel length, W is the channel width, and V_T is the threshold voltage.

Diffraction and Microscopy: Polarized optical micrographs of SiO_2 nanoparticle/TIPS pentacene thin films were obtained with a Nikon OptiPhot2-POL polarized optical microscope. Grazing-incidence X-ray diffraction was performed with an X'Pert PRO MPD Diffractometer using Cu Kα radiation. TEM images were obtained using a Hitachi HF3300 at 300 kV. Unlike films that served as the transistor active layers, TEM samples were prepared by drop casting from a much more dilute solution (0.1 wt% total solid content) onto amorphous carbon-coated copper grids to yield thin films that are suitable for imaging by transmission electron microscopy. A Zeiss Merlin SEM was used for cross-sectional imaging at 500–1000 V with the charge compensation mode to avoid electron beam damage to the TIPS pentacene active layer. A tilt angle of 16.6° was used for edge imaging.

Acknowledgements

D.L. and Z.H. acknowledge support provided from the University of Alabama. JC and SMK acknowledge the support from a DOE Laboratory Directed Research and Development (LDRD) award (#5388). This research was partially conducted at the Center for Nanophase Materials Sciences, which is sponsored at Oak Ridge National Laboratory by the Division of Scientific User Facilities, U.S. Department of Energy. Electron microscopy was conducted at the SHaRE User Facility, which is also sponsored by the Division of Scientific User Facilities, U.S. Department of Energy.

Received: December 18, 2010
Revised: March 11, 2011
Published online: July 7, 2011

[1] H. Sirringhaus, *Adv. Mater.* **2005**, *17*, 2411.
[2] G. H. Gelinck, H. E. A. Huitema, E. Van Veenendaal, E. Cantatore, L. Schrijnemakers, J. Van der Putten, T. C. T. Geuns, M. Beenhakkers, J. B. Giesbers, B. H. Huisman, E. J. Meijer, E. M. Benito, F. J. Touwslager, A. W. Marsman, B. J. E. Van Rens, D. M. DeLeeuw, *Nat. Mater.* **2004**, *3*, 106.
[3] E. J. Meijer, D. M. De Leeuw, S. Setayesh, E. Van Veenendaal, B. H. Huisman, P. W. M. Blom, J. C. Hummelen, U. Scherf, T. M. Klapwijk, *Nat. Mater.* **2003**, *2*, 678.
[4] D. W. Li, L. J. Guo, *Appl. Phys. Lett.* **2006**, *88*, 3.
[5] D. W. Li, L. J. Guo, *J. Phys. D, Appl. Phys.* **2008**, *41*, 7.
[6] J. E. Anthony, J. S. Brooks, D. L. Eaton, S. R. Parkin, *J. Am. Chem. Soc.* **2001**, *123*, 9482.
[7] S. K. Park, D. A. Mourey, J. I. Han, J. E. Anthony, T. N. Jackson, *Org. Electron.* **2009**, *10*, 486.
[8] X. R. Li, B. K. C. Kjellander, J. E. Anthony, C. W. M. Bastiaansen, D. J. Broer, G. H. Gelinck, *Adv. Funct. Mater.* **2009**, *19*, 3610.
[9] C. W. Sele, B. K. C. Kjellander, B. Niesen, M. J. Thornton, J. van der Putten, K. Myny, H. J Wondergem, A. Moser, R. Resel, A. van Breemen, N. van Aerle, P. Heremans, J.E. Anthony, G. H. Gelinck, *Adv. Mater.* **2009**, *21*, 4926.
[10] S. K. Park, T. N. Jackson, J. E. Anthony, D. A. Mourey, *Appl. Phys. Lett.* **2007**, *91*.
[11] J. H. Chen, S. Subramanian, S. R. Parkin, M. Siegler, K. Gallup, C. Haughn, D. C. Martin, J. E. Anthony, *J. Mater. Chem.* **2008**, *18*, 1961.
[12] R. L. Headrick, S. Wo, F. Sansoz, J. E. Anthony, *Appl. Phys. Lett.* **2008**, *92*, 3.
[13] J. H. Chen, C. K. Tee, M. Shtein, D. C. Martin, J. Anthony, *Org. Electron.* **2009**, *10*, 696.
[14] T. Ohe, M. Kuribayashi, R. Yasuda, A. Tsuboi, K. Nomoto, K. Satori, M. Itabashi, J. Kasahara, *Appl. Phys. Lett.* **2008**, 93.
[15] J. Kang, N. Shin, D. Y. Jang, V. M. Prabhu, D. Y. Yoon, *J. Am. Chem. Soc.* **2008**, *130*, 12273.
[16] J. Smith, R. Hamilton, I. McCulloch, M. Heeney, J. E. Anthony, D. D. C. Bradley, T. D. Anthopoulos, *Synth. Met.* **2009**, *159*, 2365.
[17] R. Hamilton, J. Smith, S. Ogier, M. Heeney, J. E. Anthony, I. McCulloch, J. Veres, D. D. C. Bradley, T. D. Anthopoulos, *Adv. Mater.* **2009**, *21*, 1166.
[18] J. Smith, R. Hamilton, I. McCulloch, N. Stingelin Stutzmann, M. Heeney, D. D. C. Bradley, T. D. Anthopoulos, *J. Mater. Chem.* **2010**, *20*, 2562.
[19] F. Croce, G. B. Appetecchi, L. Persi, B. Scrosati, *Nature* **1998**, *394*, 456.
[20] M. B. Madec, D. Crouch, G. R. Llorente, T. J. Whittle, M. Geoghegan, S. G. Yeates, *J. Mater. Chem.* **2008**, *18*, 3230.
[21] J. H. Chen, D. C. Martin, J. E. Anthony, *J. Mater. Res.* **2007**, *22*, 1701.
[22] J. H. Chen, J. Anthony, D. C. Martin, *J. Phys. Chem. B* **2006**, *110*, 16397.
[23] J. H. Chen, C. K. Tee, M. Shtein, J. Anthony, D. C. Martin, *J. Appl. Phys.* **2008**, 103.
[24] J. H. Chen, C. K. Tee, J. Y. Yang, C. Shaw, M. Shtein, J. Anthony, D. C. Martin, *J. Polym. Sci., Part B Polym. Phys.* **2006**, *44*, 3631.
[25] J. H. Chen, C. K. Tee, J. Y. Yang, C. Shaw, M. Shtein, D. C. Martin, J. Anthony, *J. Polym. Sci., Part B Polym. Phys.* **2008**, *46*, 1878.